

Spin-chirality decoupling and critical properties of a two-dimensional fully frustrated XY model

Soichirou Okumura, Hajime Yoshino and Hikaru Kawamura

Department of Earth and Space Science, Faculty of Science, Osaka University, Toyonaka 560-0043, Japan

(Dated: December 3, 2018)

We study the ordering of the spin and the chirality in the fully frustrated XY model on a square lattice by extensive Monte Carlo simulations. Our results indicate unambiguously that the spin and the chirality exhibit separate phase transitions at two distinct temperatures, *i.e.*, the occurrence of the spin-chirality decoupling. The chirality exhibits a long-range order at $T_c = 0.45324(1)$ via a second-order phase transition, where the spin remains disordered with a finite correlation length $\xi_s(T_c) \sim 120$. The critical properties of the chiral transition determined from a finite-size scaling analysis for large enough systems of linear size $L > \xi_s(T_c)$ are well compatible with the Ising universality. On the other hand, the spin exhibits a phase transition at a lower temperature $T_s = 0.4418(5)$ into the quasi-long-range-ordered phase. We found $\eta(T_s) = 0.201(1)$, suggesting that the universality of the spin transition is different from that of the conventional Kosterlitz-Thouless (KT) transition.

PACS numbers: 75.10.Hk, 74.81.Fa, 74.25.Qt

I. INTRODUCTION

Fully frustrated XY (FFXY) model is a basic statistical mechanical model of geometrically frustrated systems [1, 2]. An example is the antiferromagnetic XY spin system on the two-dimensional (2D) triangular lattice [3]. Another realization is a Josephson junction array (JJA) on the square lattice under an external magnetic field such that the flux density per plaquette is $f = 1/2$ [4, 5]. These systems possess an Ising-like Z_2 symmetry with respect to global spin reflections in spin space and a continuous $U(1)$ symmetry with respect to global spin rotations in spin space.

The ground state of the model is characterized by the opposite sense of the chirality. The chirality is an Ising-like variable taking either plus or minus corresponding to the right- and left-handed noncollinear spin structure [1]. More precisely, in the ground state of the model, the chirality exhibits a checker-board-like pattern much as in the antiferromagnetic Ising model on the square lattice. Since the chirality changes its sign with respect to global spin reflections in spin space, the Z_2 spin-reflection symmetry is broken in the ground state of the model. Then, by an analogy to the 2D Ising model, it would be natural to expect that the ordering of the chirality takes place at a finite critical temperature T_c . Concerning the continuous $U(1)$ spin symmetry, although the Mermin-Wagner theorem inhibits the onset of a true spin long-range order at any finite temperature [6], a finite-temperature transition into a quasi-long-range-ordered state like the Kosterlitz-Thouless (KT) transition [7] is still expected to occur.

A central issue in the studies of the FFX model, since the seminal work by Teitel and Jayaprakash [2], has been to clarify how these two distinct types of orderings take place. An interesting possibility among others, which has attracted researchers for decades, is that even at the temperature where the chirality establishes a long-range

order the spin (superconducting phase in case of the JJA) may remain disordered due to thermally excited, unbound vortices. Then, the orderings of the chirality and of the spin take place at two separate temperatures $T = T_c$ and $T = T_s$ such that $T_c > T_s$. We emphasize that the possibility of such a “spin-chirality decoupling” is a basic general problem in the studies of frustrated magnets including spin glasses [8]. The universality of the two transitions is also an interesting issue. However, the separation between T_c and T_s in the present system is extremely small, if any, which makes the solution of this problem technically difficult in spite of intensive studies done for more than two decades [9–35].

Under such circumstances, the purpose of the present paper is to clarify the nature of the phase transitions of the 2D FFX model by performing extensive Monte Carlo (MC) simulations for systems as large as up to $L \sim O(10^3)$. As was recently suggested by Hasenbusch, Pelissetto and Vicari (HPV) [21, 22], such large system sizes are needed to extract asymptotic crucial properties of the system. Although our system size is comparable to Hsenbusch *et al*, we study various physical quantities including those which were not studied in Refs.[21, 22]. Namely, in addition to the Binder parameters, the correlation lengths and the helicity modulus studied in Refs.[21, 22], we also investigate the specific heat, the chiral susceptibility and the vorticity modulus [36, 37] in order to shed further light on the ordering of the model. Furthermore, Refs.[21, 22] restricted their study just to the transition point, whereas we study an explicit temperature dependence of various physical quantities in a finite temperature range around the transition point(s).

Then, we have found convincing evidence that the two phase transitions take place at mutually close but two distinct temperatures. We have also found that the critical properties of the chiral transition are well compatible with the Ising universality class. We corroborate

Refs.[21, 22] in these conclusions. On the other hand, we have found that the universality of the spin transition is not compatible with the standard KT transition, a conclusion different from that of Refs.[21, 22].

The organization of the paper is as follows. In the next section, we introduce our model and explain the method of our simulations together with various physical observables we calculate. In sec. III, we present and discuss the results of our MC simulation. Finally in sec. IV, we conclude with a summary and some additional discussions. In appendix A, some details of the coulomb-gas representation of the vorticity modulus are given.

II. MODEL AND METHOD

We study the fully frustrated XY (FFXY) model on a square lattice of size $N = L \times L$. We label the sites of the square lattice as $i = 1, 2, \dots, N$ and denote their x and y -coordinates as $x_i = 1, 2, \dots, L$ and $y_i = 1, 2, \dots, L$. Similarly, we label the plaquettes as $n = 1, 2, \dots, N$ and denote their coordinates as $x_n = 1, 2, \dots, L$ and $y_n = 1, 2, \dots, L$.

The Hamiltonian of the model is given by,

$$H = - \sum_{\langle i,j \rangle} J_{ij} \vec{S}_i \cdot \vec{S}_j, \quad (1)$$

where $\vec{S}_i = (S_i^x, S_i^y) = (\cos \theta_i, \sin \theta_i)$ ($0 \leq \theta_i < 2\pi$) is the two-component spin variable at the site i . The summation $\langle ij \rangle$ is taken over all nearest-neighboring sites. The interaction bond takes two possible values $J_{ij} = \pm J$ such that every plaquette on the square lattice is frustrated, *i.e.*, the product of J_{ij} around each plaquette is $\prod \text{sign}(J_{ij}) = -1$. In the following, we measure the (reduced) temperature $k_B T/J$ in a unit with $k_B/J = 1$. We denote the thermal averages as $\langle \dots \rangle$.

A. Chirality-related observables

Let us introduce first physical observables associated with the chirality. We define the local chirality at a plaquette n by,

$$\kappa_n = \frac{1}{2\sqrt{2}} \sum \text{sign}(J_{ij}) \sin(\theta_i - \theta_j), \quad (2)$$

where the sum is taken over the four bonds around the plaquette. The normalization factor is chosen such that the absolute value of the chirality becomes unity in the ground state. The checker-board-like order of the chirality can be detected though a ‘staggered-chirality’,

$$m_c = \frac{1}{N} \sum_{n=1}^N (-1)^{x_n+y_n} \kappa_n. \quad (3)$$

We study the onset of the chiral order via the chiral Binder parameter,

$$g_c = \frac{3}{2} \left(1 - \frac{\langle m_c^4 \rangle}{2 \langle m_c^2 \rangle^2} \right), \quad (4)$$

and the chiral correlation length,

$$\xi_c = \frac{1}{2 \sin(\pi/L)} \sqrt{\frac{\langle |m_c(\vec{0})|^2 \rangle}{\langle |m_c(\vec{q}_{\min})|^2 \rangle} - 1}, \quad (5)$$

where

$$m_c(\vec{q}) = \frac{1}{N} \sum_{n=1}^N (-1)^{x_n+y_n} e^{i\vec{q} \cdot \vec{r}_n} \kappa_n. \quad (6)$$

is the Fourier transform of the staggered-chirality where $\vec{q}_{\min} = \frac{2\pi}{L} \vec{e}_x$ and $\vec{r}_n = (x_n, y_n)$.

In addition, we examine the staggered chiral susceptibility defined by,

$$\chi_c = N \beta \langle m_c^2 \rangle, \quad (7)$$

where β is the inverse temperature.

B. Spin-related observables

Next, we introduce the physical quantities associated with the spin. The spin order parameter is defined via the sublattice magnetization. The square lattice is decomposed into four sublattices, and the sublattice magnetization is defined by,

$$m_{s,\alpha} = \frac{1}{N/4} \left| \sum_{i \in \text{sublattice } \alpha} \vec{S}_i \right|, \quad (8)$$

where $\alpha = 1, 2, 3, 4$ denotes each sublattice.

In 2D, the spin order parameter should vanish in the thermodynamic limit $N \rightarrow \infty$ at any finite temperature. However, the spin may still establish a *quasi*-long-range order below a finite transition temperature T_s . To detect such a spin order, we measure the spin Binder parameter,

$$g_s = \frac{1}{4} \sum_{\alpha=1}^4 \left(2 - \frac{\langle m_{s,\alpha}^4 \rangle}{\langle m_{s,\alpha}^2 \rangle^2} \right), \quad (9)$$

and the spin correlation length,

$$\xi_s = \frac{1}{4} \sum_{\alpha=1}^4 \frac{1}{2 \sin(\pi/L)} \sqrt{\frac{\langle m_{s,\alpha}(\vec{0})^2 \rangle}{\langle m_{s,\alpha}(\vec{q}_{\min})^2 \rangle} - 1}, \quad (10)$$

where

$$m_{s,\alpha}(\vec{q}) = \frac{1}{N/4} \left| \sum_{i \in \text{sublattice } \alpha} e^{i\vec{q} \cdot \vec{r}_i} \vec{S}_i \right|, \quad (11)$$

and $\vec{q}_{\min} = (2\pi/L, 0)$. We also calculate the sublattice spin susceptibility defined by,

$$\chi_s = N \sum_{\alpha=1}^4 \beta \langle m_{s,\alpha}^2 \rangle. \quad (12)$$

In addition, we study the helicity modulus and the vorticity modulus which detect the rigidity of the system against appropriate spin deformations. The two quantities are related but have physically different meanings as explained below.

The helicity modulus Υ measures the rigidity of the system against an infinitesimal uniform twist of the spins $\Delta\theta$ applied on the boundary. More precisely, it is defined through the change of the total free energy ΔF with respect to an infinitesimal twist on the spin configuration along, say, y -axis $\theta_i - \theta_{i'} \rightarrow \theta_i - \theta_{i'} + (\Delta\theta/L)$ where i' is the nearest neighbour site of site i along the $+y$ direction. One readily finds,

$$\Delta F = \Upsilon(\Delta\theta)^2 + O(\Delta^4). \quad (13)$$

The helicity modulus is then given by,

$$\Upsilon = \frac{1}{N} \left[\left\langle \sum_i J_{ii'} \cos(\theta_i - \theta_{i'}) \right\rangle - \beta \left\langle \sum_i J_{ii'} \sin(\theta_i - \theta_{i'}) \right\rangle^2 \right]. \quad (14)$$

On the other hand, the vorticity modulus [36, 37] measures the rigidity of the system against a creation of an extra vortex. Disregarding the discrete nature of the vorticity, we consider an *infinitesimal* increase of the vorticity represented by the phase differences $\theta_i - \theta_j \rightarrow \theta_i - \theta_j + m\phi_{ij}$ across each bond $\langle ij \rangle$ where m is assumed to be small. Here $\phi_{ij} = -\phi_{ji}$ is the solid angle between site i and j with respect to an arbitrarily chosen origin in the system where the core of the vortex is supposed to be located. In practice, we define the solid angle as $\phi_{ij} = \hat{e}_{ij} \cdot \hat{\phi}_{ij} / \sqrt{x_i^2 + y_i^2}$. Here \hat{e}_{ij} is the unit vector connecting the neighboring sites i and j , and $\hat{\phi}_{ij}$ is a unit vector tangential to the circular path passing through the site i enclosing the origin. One readily finds that the free-energy increase can be expressed as,

$$\Delta F = Vm^2 + O(m^4), \quad (15)$$

with

$$V = \left\langle \sum_{\langle i,j \rangle} J_{ij} \phi_{ij}^2 \cos(\theta_i - \theta_j) \right\rangle - \beta \left\langle \sum_{\langle i,j \rangle} J_{ij} \phi_{ij} \sin(\theta_i - \theta_j) \right\rangle^2. \quad (16)$$

For large enough systems, we expect the scaling behaviour,

$$V(T, L) \approx c(T) + v(T) \ln L, \quad (17)$$

where $v(T)$ is the vorticity modulus. In appendix A, we present a coulomb-gas representation of the vorticity modulus which might provide some insight into the physical meaning of this quantity.

In practice, we evaluate the vorticity modulus $v(T)$ in two different ways. The first way is to define the effective vorticity modulus by,

$$v_1(T, L) = \frac{V(T, L)}{\ln L}, \quad (18)$$

and examine its $L \rightarrow \infty$ limit. The second way is to define the effective vorticity modulus using the data at two different system sizes L_1 and L_2 [37],

$$v_2(T, L_1, L_2) = \frac{V(T, L_1) - V(T, L_2)}{\ln(L_1/L_2)}, \quad (19)$$

and examine its $L_1, L_2 \rightarrow \infty$ limit. The advantage of v_2 compared with the first one $v_1(T)$ is that the anticipated constant term $c(T)$ in Eq. (17) is cancelled so that a finite-size correction becomes smaller.

C. Monte Carlo simulations

We use a Monte Carlo method which combines the Metropolis method and the over-relation method [38]. Within a single Monte Carlo Step (MCS), the spins are updated by one sweep using the Metropolis method which is followed by three consecutive over-relaxation sweeps. System sizes of $L = 32, 64, 128, 256, 512, 1024$ plus $L = 384, 768$ under periodic boundary conditions are studied. We use the histogram method to evaluate physical quantities around the critical temperature. Typical MC steps used for equilibration and measurements are 10^8 MCS for $L = 512, 768, 1024$ around the chiral transition temperature and 5×10^6 MCS around the spin transition temperature.

III. RESULTS

In this section, we present the results of our MC simulations.

A. Specific heat

We begin with the specific heat $C = \beta^2(\langle H^2 \rangle - \langle H \rangle^2)$. As shown in Fig. 1(a), the specific heat exhibits a sharp peak as a function of the temperature at $T = T_{\text{peak}}(L)$. The height of the peak increases with increasing L , suggesting the occurrence of a second-order phase transition. Meanwhile, there is no indication of other phase transitions. This could be explained if one recalls that the expected spin transition might be of the KT-type which is known not to accompany a distinct anomaly in the

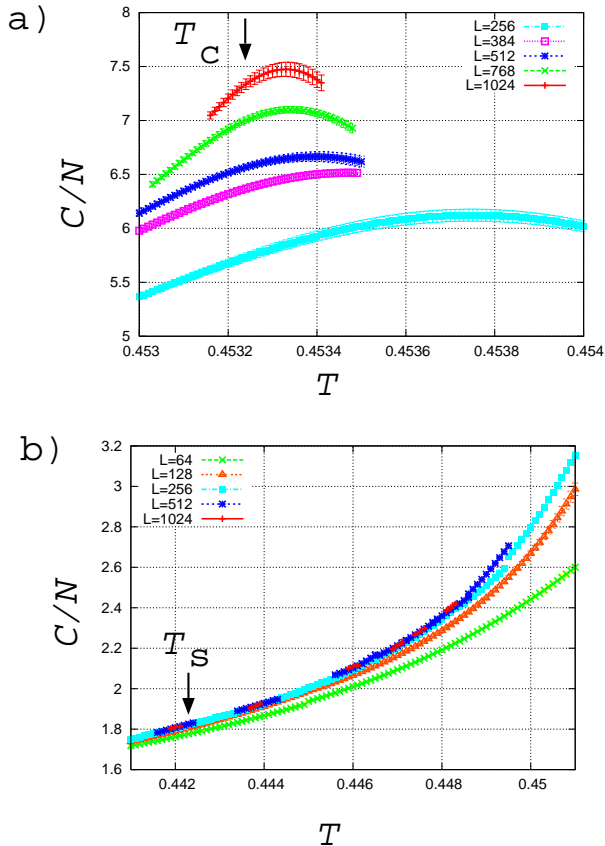


FIG. 1: The temperature dependence of the specific heat per spin. The panels a) and b) show the data around the chiral transition temperature T_c and spin transition temperature T_s , respectively. The arrows indicate the estimated transition temperature for the chirality T_c , and for the spin T_s .

specific heat. Therefore it is natural to expect that the specific-heat-peak is associated with the chiral transition.

In order to estimate the bulk chiral transition temperature T_c , we show in Fig. 3 the size dependence of the specific-heat-peak temperature $T_{\text{peak}}(L)$. Interestingly, the system-size dependence of the peak temperature $T_{\text{peak}}(L)$ exhibits a crossover behaviour around $L = L_\times \sim 200$: For sizes smaller than $L_\times \sim 200$, $T_{\text{peak}}(L)$ exhibits a near-linear dependence, while for sizes greater than L_\times , $T_{\text{peak}}(L)$ exhibits another near-linear dependence but with a different slope. By making a linear extrapolation of $T_{\text{peak}}(L)$ for large enough system sizes $L > L_\times \sim 200$, we get an estimate of the chiral critical temperature, $T_c = 0.45324(1)$: See Fig. 3(b). It implies that the long-range order of the chirality is established at $T_c = 0.45324(1)$ via a second-order phase transition. Since the finite-size scaling ansatz implies $T_{\text{peak}}(L) \approx T_c + \text{const}L^{-1/\nu_c}$ where the critical exponent ν_c describes the divergence of the chiral correlation length, the chiral transition is characterized by $\nu_c \simeq 1$, which is consistent with the the Ising universality class. Our present estimate of T_c and the Ising nature of the

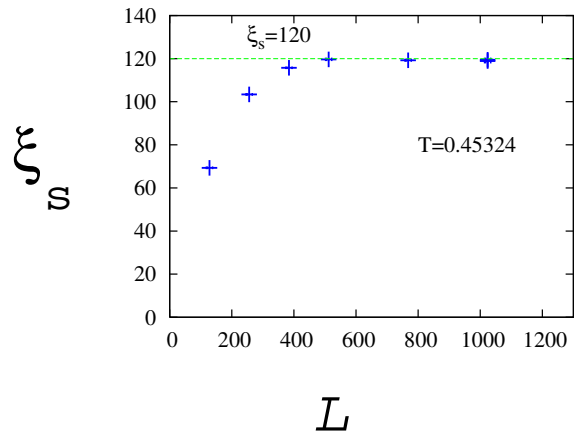


FIG. 2: Spin correlation length $\xi_s(T, L)$ measured at the chiral transition temperature $T_c = 0.45324$ for various system sizes.

transition are consistent with the results of many recent works, particularly with the most recent result by Hasenbusch et al who gave $T_c = 0.45324(1)$ [21, 22].

Now we turn to the issue of the crossover observed around $L_\times \sim 200$, which is likely to reflect a change in the nature of the ordering of the spin. In the inset of Fig. 2, we show the size dependence of the spin correlation length ξ_s at the chiral transition point $T_c = 0.45324$ determined above. As can be seen from the figure, $\xi_s(T_c)$ tends to saturate for large enough sizes of $L > 200$, yielding $\xi_s(T_c) \sim 120$, which is indeed comparable to the crossover length scale $L_\times \sim 200$ determined above. This result indicates that the observed size-crossover reflects the change in the ordering behavior of the system from the ‘spin-chirality coupling’ regime where the spin correlation dominates the ordering to the ‘spin-chirality decoupling’ regime where the chiral correlation outgrows the spin correlation and dominates the ordering of the system.

The universality of the chiral transition of the 2D FFX model has been a matter of intense debate in the previous studies. Most probably, the source of the confusion is this size-crossover effect associated with the spin-chirality coupling/decoupling. If one looked at small enough systems compared with the crossover length L_\times , one should find an effective ν -exponent close to unity as demonstrated in Fig. 1(a), which would suggest the Ising universality. This was actually observed in simulations in early days [3, 24], where system sizes in the range $10 < L < 50$ were studied. However, if one focused on intermediate length scales around L_\times , one would find $\nu < 1$, which would suggest the non-Ising universality [13, 14, 18–20, 25]. Then, at length scales sufficiently larger than L_\times , the effective ν -exponent would become closer to unity again [21, 22]. Our present estimates of T_c and ν are in perfect agreement with the recent estimates of Hasenbusch *et al* [21, 22].

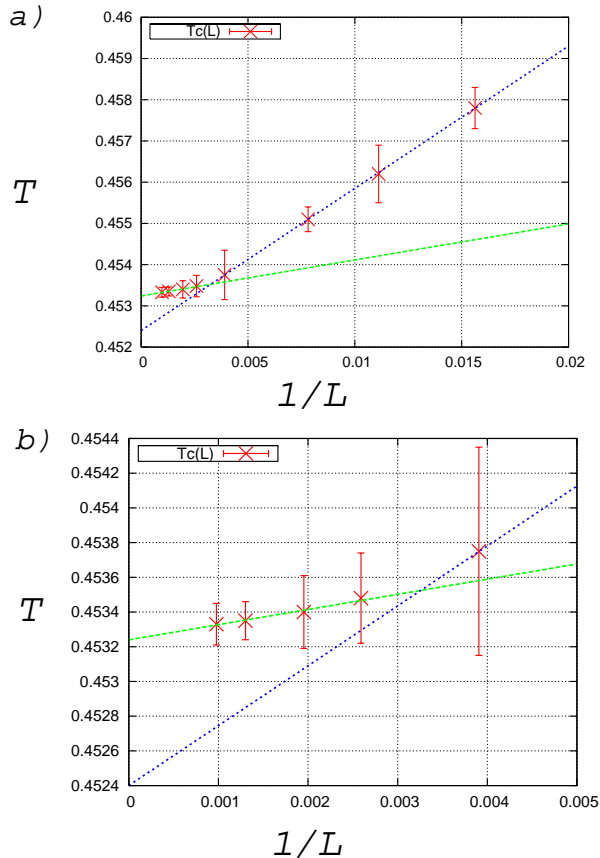


FIG. 3: The specific-heat-peak temperature $T_{\text{peak}}(L)$ plotted versus the inverse linear size $1/L$, for (a) all sizes investigated, and for (b) larger sizes. The straight lines represent linear fits of the data at smaller sizes $L < 200$, and at larger sizes $L > 200$.

To get more insight into the ordering process of the model, we proceed to analyze in the next subsections physical quantities which are directly related to the order parameters.

B. Chirality-related quantities

In this subsection, we examine the ordering of the chirality. As shown in Fig. 4(a), the chiral Binder parameter $g_c(T, L)$ of different sizes exhibit clear crossings. The scaled correlation-length, or the chiral correlation-length ratio $\xi_c(T, L)$, also exhibits similar crossings as shown in Fig. 4(b).

To analyze the size dependence of the crossing points quantitatively, we label the system sizes in the ascending order $L_1 < L_2 \dots$ and plot in Fig. 5 the crossings point $T_{\text{cross}}(L)$ of the Binder parameter and of the chiral correlation-length ratio at adjacent sizes L_{n+1} and L_n as a function of the average size $L_{av} = \frac{L_{n+1} + L_n}{2}$. As in the case of the specific-heat-peak temperature, the crossing temperature $T_{\text{cross}}(L)$ of both the Binder parameter

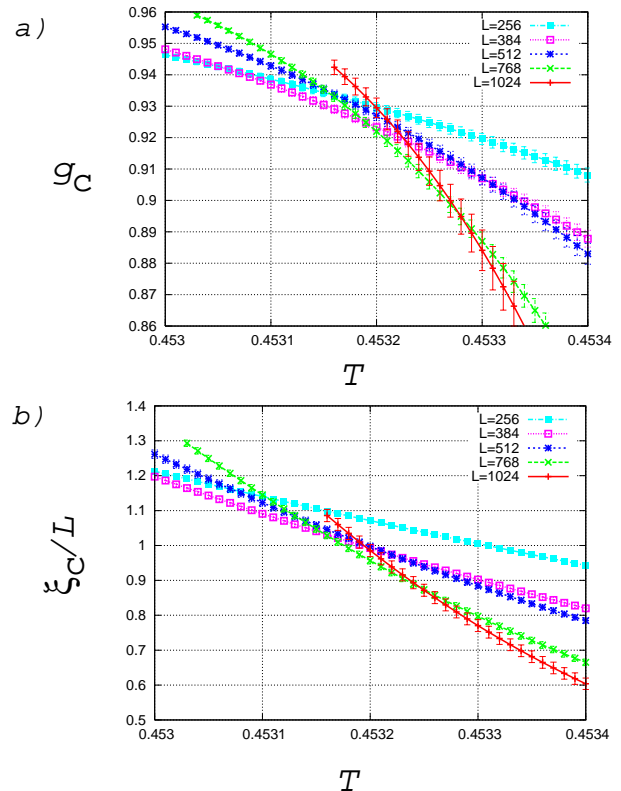


FIG. 4: The temperature dependence of (a) the chiral Binder parameter g_c , and of (b) the chiral correlation-length ratio ξ_c/L .

and the correlation-length ratio exhibits a size-crossover at around $L \sim 200$, the same crossover length observed in the specific heat, where a non-monotonic size dependence with an abrupt turnover takes place. With use of the data of larger sizes $L > L_{\times}$, the chiral transition temperature is estimated as $T_c = 0.45324(5)$, which agrees well with the estimate above obtained from the specific heat $T_c = 0.45324(1)$.

To examine the universality of the chiral transition further, we analyze the chiral susceptibility χ_c . At the chiral transition temperature T_c , a power-law behaviour $\chi_c(T_c, L) \propto L^{2-\eta_c}$ is expected with a chiral anomalous-dimension exponent η_c . We analyze the data at each temperature T shown in Fig. 6 by fitting them to the form $\chi_c(T, L) = a(T) + b(T)L^{2-\eta_{\text{eff}}(T)}$ with three fitting parameters $a(T)$, $b(T)$ and $\eta_{\text{eff}}(T)$.

The temperature dependence of the effective exponent $\eta_{\text{eff}}(T)$ is displayed in Fig. 7(a). We find that, at the chiral transition temperature $T_c = 0.45324$ estimated above, the effective exponent $\eta_{\text{eff}}(T)$ takes a value $0.25(3)$. This observation is consistent with the expected Ising value $\eta = 1/4$, giving further support to the Ising nature of the chiral transition.

In Fig. 7(b), we display the temperature dependence of our another fitting parameter $a(T)$. Presumably, this parameter reflects fluctuations at short length scales where

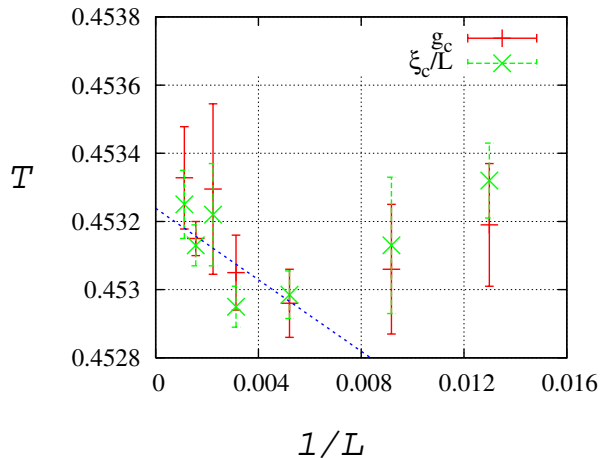


FIG. 5: Crossing temperatures of the chiral Binder parameter g_c and of the chiral correlation-length ratio ξ_c/L are plotted versus the inverse linear size $1/L$. The dashed line is a linear fit which yields $T_c = 0.45324(5)$.

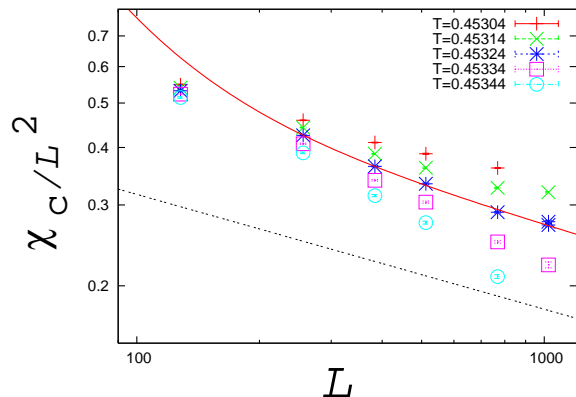


FIG. 6: The chiral susceptibility divided by L^2 is plotted versus the system size L on a log-log plot. The solid line represents a fit to the form $\chi_c(T, L) = a(T) + b(T)L^{2-\eta_{\text{eff}}(T)}$ of the data at $T = T_c = 0.45324$. For comparison, a power-law $L^{-\eta}$ behavior with the Ising exponent $\eta = 1/4$ is also shown by the dotted line.

chiral and spin orders are not separated. The increase of $a(T)$ with decreasing temperature T may be interpreted as due to the growth of the spin correlation length $\xi_s(T)$ approaching T_s .

C. Spin-related quantities

Next, we examine the ordering of the spin. The spin Binder parameter $g_s(T, L)$ and the spin correlation-length ratio $\xi_s(T, L)/L$ are shown in Fig. 8(a) and (b), respectively. Data of different sizes exhibit crossings as in the case of chirality shown in Fig. 4. From the raw data, it is already evident that the spin crossing temperatures

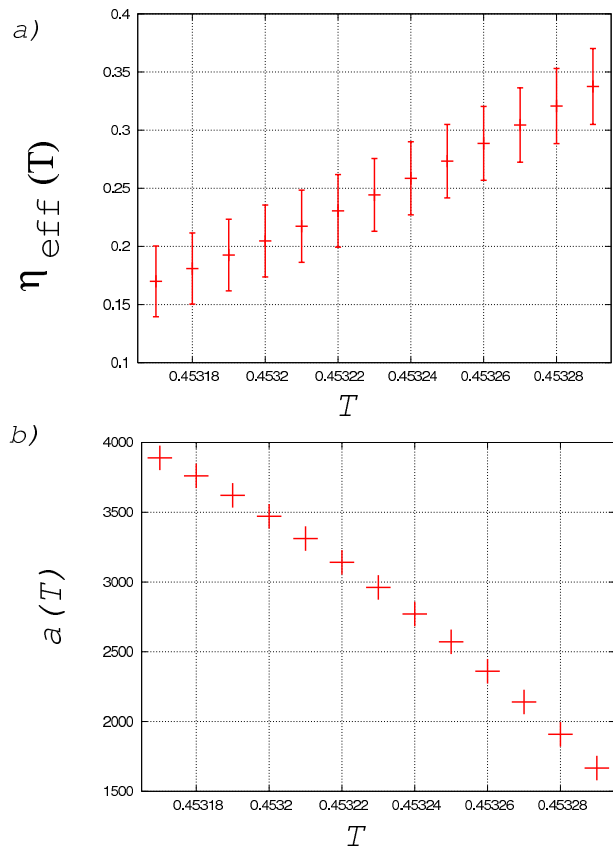


FIG. 7: The temperature dependence of the parameter values obtained in the fitting analysis of the chiral susceptibility based on the form $\chi_c(T, L) = a(T) + b(T)L^{2-\eta_{\text{eff}}(T)}$: a) the effective exponent $\eta_{\text{eff}}(T)$, and b) the constant $a(T)$.

are considerably lower than chiral transition temperature $T_c = 0.45324(1)$. It means that the chirality and the spin exhibit two separate transitions.

In addition, the raw data also suggests a qualitative difference in the nature of the orderings of the spin and the chirality. In case of the spin shown in Fig. 8, the separation between the data points of different sizes tends to become increasingly small for larger systems, exhibiting a marginal behavior, whereas in case of the chirality shown in Fig. 4 the data points of different system sizes remain well separated even for larger systems. This difference reflects the fact that, while the chirality exhibits a finite long-range order at finite temperature even in 2D, the spin cannot establish a true long-range order at finite temperature but only a quasi-long-range order.

The effective vorticity modulus v_1 and v_2 defined by Eq. (18) and Eq. (19) are displayed in Fig. 9(a) and (b), respectively. The effective vorticity modulus v_1 exhibits a stronger finite-size effect compared with v_2 , as expected. v_2 exhibit merging behaviour at low temperatures suggesting the onset of the quasi-long ranged order. Again, it can be seen that the crossing temperatures of the vorticity modulus are considerably lower than the chiral transition temperature $T_c = 0.45324(1)$.

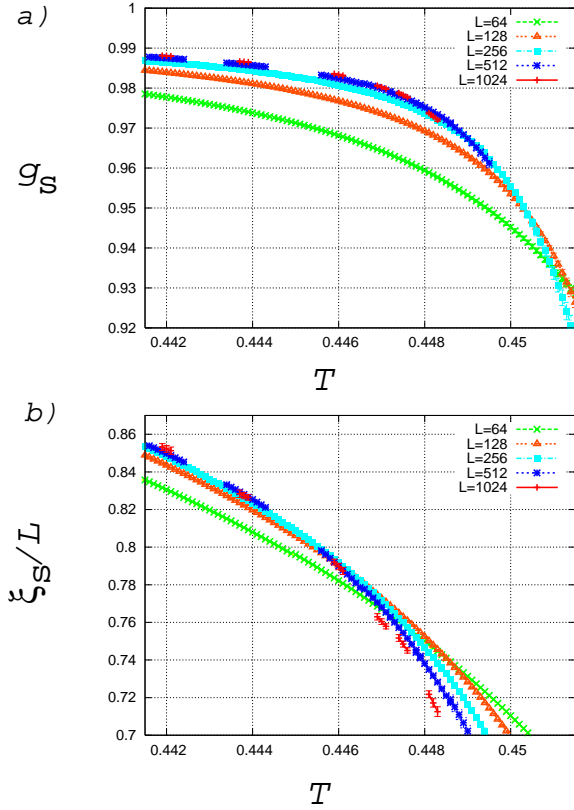


FIG. 8: The temperature dependence of (a) the spin Binder parameter g_s , and of (b) the spin correlation-length ratio ξ_s/L . Evidently the crossing temperatures are lower than the chiral transition temperature $T_c = 0.45324$.

Now we estimate quantitatively the spin transition temperature T_s based on our data of the crossing temperatures of several observables presented above. Thus, the crossing temperatures $T_{\text{cross}}(L)$ of the spin Binder parameter $g_s(T, L)$, the spin correlation-length ratio $\xi_s(T, L)/L$ and the effective vorticity modulus v_1 between the two adjacent sizes L_1 and L_2 are plotted against $1/(\ln L_{av})^2$ in Fig.10. Note that this form is motivated by the standard KT form $\xi_s \sim \exp[c/\sqrt{T - T_s}]$. From the combined fit of these data where a common spin transition temperature T_s is assumed, we get an estimate of the bulk spin transition temperature $T_s = 0.4418(5)$.

In Fig.10 we also display the size dependence of the crossing points of the spin correlation-length ratio $\xi_s(T, L)/L$ between the two sizes L and sL with $s = 2, 4, 8$ plotted as a function of $1/(\ln L)^2$. From the combined fit of these three data sets where a common spin transition temperature T_s is assumed, we get $T_s = 0.4414(3)$ which is consistent with our estimate presented above.

In order to examine the universality of the spin transition, we also analyze the sublattice spin susceptibility χ_s . At and below the spin transition temperature T_s , a power-law behaviour $\chi_s(T_c, L) \propto L^{2-\eta(T)}$ is expected with a spin anomalous-dimension exponent $\eta(T)$. We

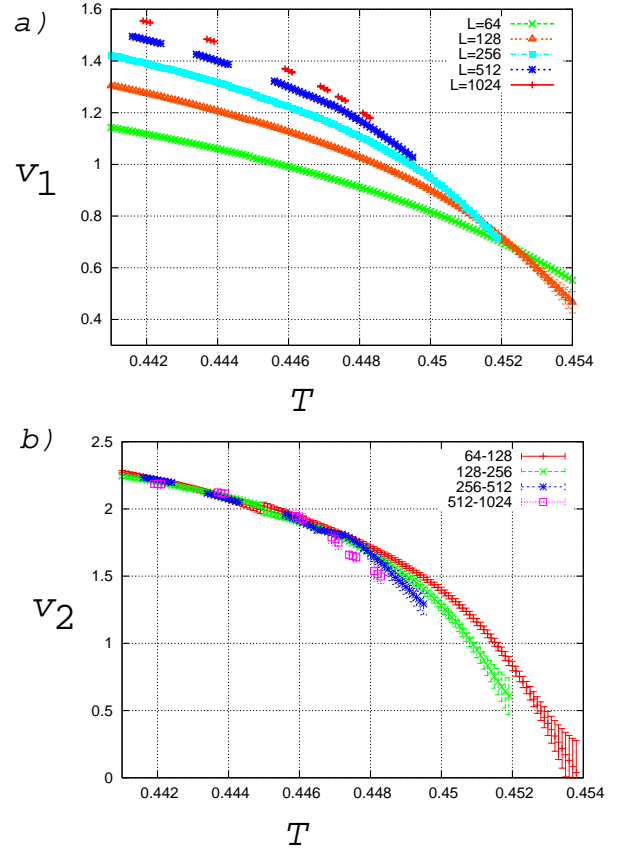


FIG. 9: The temperature dependence of the two types of the effective vorticity modulus, (a) v_1 defined by Eq. (18), and (b) v_2 defined by Eq. (19).

analyze the data shown in Fig. 11 by fitting them to the form $\chi_s(T, L) = b(T)L^{2-\eta_{\text{eff}}(T)}$ with two fitting parameters $b(T)$ and $\eta_{\text{eff}}(T)$ at each temperature T .

The temperature dependence of the effective exponent $\eta_{\text{eff}}(T)$ is displayed in Fig. 12(a). We find that, at the spin transition temperature $T_s = 0.4418(5)$ estimated above, the effective exponent $\eta_{\text{eff}}(T)$ takes a value $0.201(2)$. Remarkably, this value is significantly smaller than the value of the conventional Kosterlitz-Thouless (KT) transition $\eta = 1/4$ [7]. This observation suggests that the universality of the spin-transition of the present 2D FFX model might be different from that of the conventional KT transition.

To get further insight, we also examine the helicity modulus. In 2D XY models, the helicity modulus is expected to exhibit a discontinuous jump from zero at higher temperatures to a nonzero value $T_s/(2\pi\eta(T_s))$ at the critical temperature T_s . From the raw data displayed in Fig. 13, we extract the intersection points between the helicity-modulus data of each size and a straight line $T/(2\pi\eta(T_s))$ by setting $\eta(T_s) = 0.201(2)$ as obtained above. Then, the size dependence of the resulting intersection points is displayed in Fig. 14. Assuming that the correction term scales as $1/\ln^2(L)$, we find

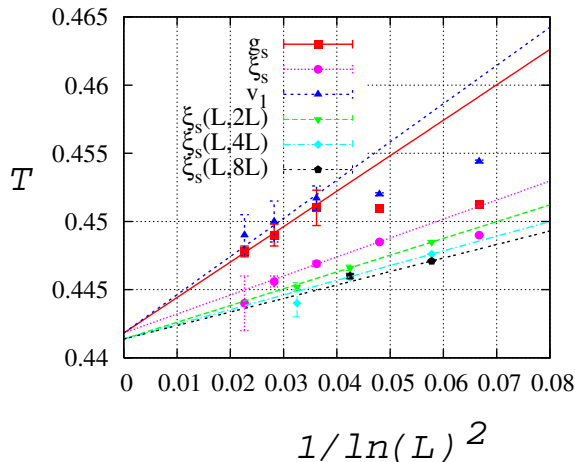


FIG. 10: Crossing temperatures of the spin Binder parameter g_s (Fig. 8(a)), of the spin correlation-length ratio ξ_s/L (Fig. 8(b)), and of the effective vorticity modulus v_1 (Fig. 9(a)) are plotted versus $(1/\ln L)^2$. L in the horizontal axis is the average system size. The combined straight-line fits for three kinds of crossing temperatures assuming a common T_s yields $T_s = 0.4418(5)$. In addition, crossing temperatures of the spin correlation-length ratio ξ_s/L between the two sizes L and sL with $s = 2, 4, 8$ are also shown as a function of $1/(\ln L)^2$. The combined fit using the last three data sets assuming a common T_s yields $T_s = 0.4414(3)$.

$T_s = 0.44185(5)$. This value of T_s is consistent with our estimate above $T_s = 0.4418(5)$ obtained from the Binder parameter, the correlation-length ratio and the vorticity modulus.

If one assumes instead the conventional KT value $\eta(T_s) = 1/4$ in the above analysis of the helicity modulus as was done in Refs.[16, 21, 22], one obtains $T_s = 0.44619(4)$ as displayed in Fig. 14. The latter value agrees well with the estimate of $T_s = 0.446$ (Ref.[16]) and $T_s = 0.4461(1)$ (Ref.[21, 22]). However, this value is not compatible with our present estimate of T_s obtained from other quantities *without assuming a specific value for the exponent $\eta(T_s)$* , $T_s = 0.4415(3)$.

Our result indicates that the jump of the helicity modulus is greater than the so-called ‘universal jump’ for the conventional KT transition [39–41]. Lee and Lee [18] made a similar observation in the FFX model on the triangular lattice. Indeed, such a possibility was mentioned occasionally since early days of research [2].

IV. SUMMARY AND DISCUSSIONS

We studied the ordering of the spin and the chirality of the 2D FFX model on the square lattice by extensive Monte Carlo simulations performed up to very large system size to circumvent crossover effects. We found the chiral transition takes place at $T_c = 0.45324(1)$, while spin transition takes place at $T_s = 0.4418(5)$. Thus, the

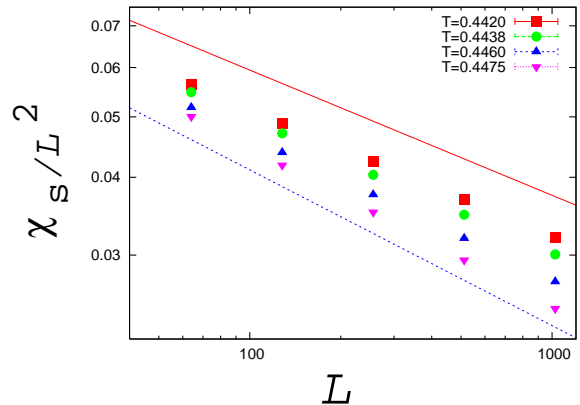


FIG. 11: The sublattice spin susceptibility divided by L^2 is plotted versus L on a log-log plot. The straight lines represent power laws $L^{-\eta}$ with $\eta = 1/4$ (green broken line) and with $\eta = 0.201$ (red solid line).

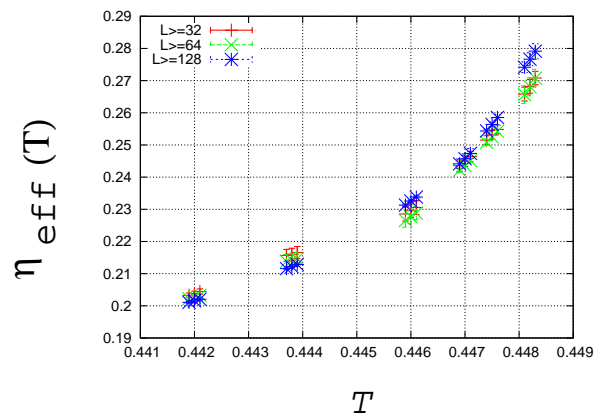


FIG. 12: The temperature dependence of the effective spin exponent $\eta_{\text{eff}}(T)$ extracted from the fitting of the sublattice spin susceptibility $\chi_s(T, L)$ to the form $\chi_s(T, L) = b(T)L^{2-\eta_{\text{eff}}(T)}$ using the data of $L \geq 32$, ≥ 64 and ≥ 128 .

model certainly exhibits the spin-chirality decoupling, where T_s lies below T_c by about 2.6%.

As pointed out by Hasenbusch *et al* [21, 22], in order to observe separation of the two transitions it is crucial to simulate large enough system sizes. In Fig. 15 we display the raw data of the correlation length of the chirality and of the spin. Evidently, the two correlation lengths are almost equal at higher temperatures $T > 0.468$, behaving side by side. This is the spin-chirality coupling behavior expected in the high-temperature regime. At lower temperatures, the bulk chiral correlation length becomes definitely longer than the bulk spin correlation length. For instance, at $T = 0.456$ we find $\xi_c \sim 65$ while $\xi_s \sim 45$. In the temperature range $T < 0.458$, we get into the spin-chirality decoupling regime. At the chiral transition temperature $T_c = 0.45324(1)$, the chiral correlation length diverges while the spin correlation length $\xi_s(T_c, L)$

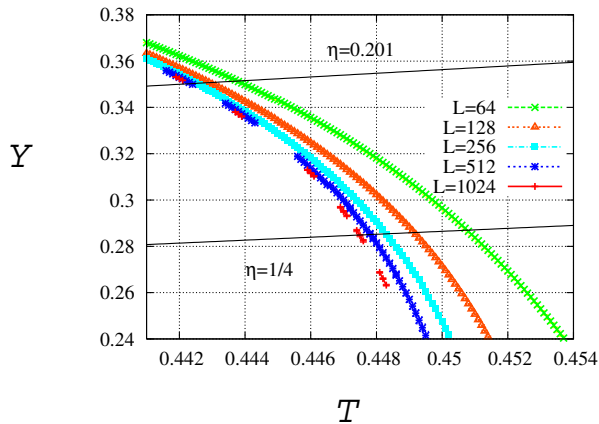


FIG. 13: The temperature dependence of the helicity modulus. The straight lines represent $T/(2\pi\eta)$ with $\eta = 0.201$ and $1/4$.

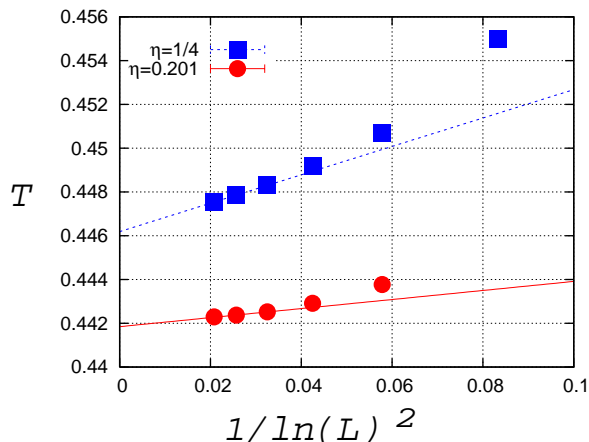


FIG. 14: Intersection points of the helicity modulus obtained by assuming $\eta(T_s) = 0.201$ and $1/4$ are plotted versus $1/(\ln L)^2$. The straight lines represent the linear fits of the data.

stays at a finite value around 120 as shown in the inset of Fig. 15.

The universality class of each transition was also studied. The universality class of the chiral transition is well compatible with the Ising universality. On the other hand, the universality class of the spin transition is different from the conventional KT transition.

Possibility of the non-universal jump of the helicity modulus was pointed out on the general ground of a refined renormalization-group scheme by Minnhagen [42] and was argued to be relevant to the fully frustrated XY model [26]. However the true connection to the frustration system was not necessarily clear. The spin and the chirality orderings of the fully frustrated XY model was also studied by Choi and Stroud by means of a renormalization group analysis of the coupled XY model which is believed to be essentially equivalent to the FFX model

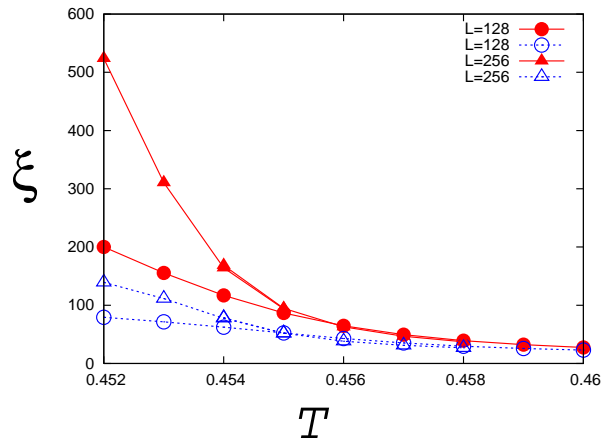


FIG. 15: Direct comparison of the chiral and the spin correlation lengths for the sizes $L = 128$ and 256 . The full/open symbols are the finite-size data of the chiral/spin correlation length, respectively.

[33]. The possible non-universal jump of the helicity modulus was suggested [34, 35]. The latter RG scheme [33–35] is quite appealing since it aimed at studying the ordering behaviours of both the chirality and the spin in a unified manner. However, the assumption underlying the derivation of the RG equations, i. e. the smallness of the fugacity of the *both* the usual spin vortices and extra charges responsible for the ordering of the chirality, each being justifiable in the low-temperature and in the high-temperature limits, cannot be satisfied asymptotically upon renormalization at any temperature. It will be very interesting to investigate further the nature of the spin transition in the presence of the chiral long-ranged order, which is not considered in conventional theories for the KT transition.

The numerical calculations were carried out partly on SX8 at Yukawa Institute of Theoretical Physics in Kyoto University and on SX-8R at the Cybermedia Center in Osaka University. This work is supported by Grant-Aid for Scientific Research on Priority Areas “Novel States of Matter Induced by Frustration” (19052006).

Appendix A: Vorticity modulus in the coulomb gas representation

In order to get some insight into the meaning of the vorticity modulus, we derive in this appendix its coulomb representation.

The partition function of our model can be represented as,

$$Z = \int \prod_i d\theta_i \prod_{\langle ij \rangle} e^{-\beta E_{ij}(\{\theta_{ij}\}, \{A_{ij}\})}, \quad (\text{A1})$$

with

$$E_{ij}(\{\theta_{ij}\}, \{A_{ij}\}) = -J \cos(\theta_i - \theta_j - A_{ij}), \quad (\text{A2})$$

The parameter A_{ij} (vector potential) is understood as an anti-symmetric tensor,

$$A_{ij} = -A_{ji}. \quad (\text{A3})$$

For a ferromagnetic/antiferromagnetic bond, we choose $A_{ij} = 0/\pi$, respectively.

We consider the change in the free energy by an *infinitesimal* increase of the vorticity m ,

$$V = \left. \frac{\partial^2 F(m)}{\partial m^2} \right|_{m=0}, \quad (\text{A4})$$

where $F(m)$ is the free-energy of the system with a modified vector potential,

$$A_{ij} \rightarrow A_{ij} + m\phi_{ij}, \quad (\text{A5})$$

where ϕ_{ij} is an ‘angle’ between the sites i and j with respect to the origin O, as shown in Fig. 16. We set,

$$\phi_{ij} = -\phi_{ji}. \quad (\text{A6})$$

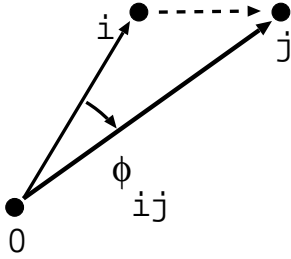


FIG. 16: Solid angle ϕ_{ij} between sites i and j with respect to the origin O.

By the standard steps of mappings [40], we find that the partition function of the system can be represented as,

$$Z = Z_{\text{sw}} \prod_{\vec{n}} \sum_{q_{\vec{n}}=-\infty}^{\infty} e^{-\beta \mathcal{H}(\{\tilde{q}_{\vec{n}}\})}, \quad (\text{A7})$$

where Z_{sw} is the contribution from spin-waves and $\mathcal{H}(\{\tilde{q}_{\vec{n}}\})$ is an effective charge Hamiltonian for the charge variables $\tilde{q}_{\vec{n}}$ defined on the dual lattice with its lattice points $\vec{n} = (x_n, y_n)$ located at the centers of the plaquettes of the original lattice,

$$\tilde{q}_{\vec{n}} = q_{\vec{n}} + b_{\vec{n}}. \quad (\text{A8})$$

Here $q_{\vec{n}}$ is an integer and $b_{\vec{n}}$ is a ‘flux’ defined by

$$b_{\vec{n}} = \frac{1}{2\pi} \sum_{\langle ij \rangle \text{ around } \vec{n}} A_{ij}, \quad (\text{A9})$$

where the sum is taken around the plaquette at \vec{n} in a counter-clockwise direction.

One can see that the contribution from the additional term $m\phi_{ij}$ in the vector potential Eq. (A5) to the flux $b_{\vec{n}}$ is zero almost everywhere except at the origin $\vec{n} = \vec{0}$;

$$b_{\vec{n}} = m\delta_{\vec{n},\vec{0}} + \frac{1}{2\pi} \sum_{\langle ij \rangle \text{ around } \vec{n}} A_{ij}. \quad (\text{A10})$$

Here it is made evident that m can be interpreted indeed as an *infinitesimal* charge or vorticity.

We then find,

$$\begin{aligned} \left. \frac{\partial^2(-\beta F)}{\partial m^2} \right|_{m=0} &= \left\langle \frac{\partial^2(-\beta \mathcal{H})}{\partial(\tilde{q}_{\vec{0}})^2} \right\rangle_c \\ &+ \left\langle \left(\frac{\partial(-\beta \mathcal{H})}{\partial(\tilde{q}_{\vec{0}})} \right)^2 \right\rangle_c - \left\langle \frac{\partial(-\beta \mathcal{H})}{\partial(\tilde{q}_{\vec{0}})} \right\rangle_c^2, \end{aligned} \quad (\text{A11})$$

where

$$\langle \dots \rangle_c \equiv \frac{\prod_{\vec{n}} \sum_{q_{\vec{n}}=-\infty}^{\infty} \dots e^{-\beta \mathcal{H}(\{\tilde{q}\})}}{\prod_{\vec{n}} \sum_{q_{\vec{n}}=-\infty}^{\infty} e^{-\beta \mathcal{H}(\{\tilde{q}\})}}. \quad (\text{A12})$$

An explicit form of the charge Hamiltonian $\mathcal{H}(\{\tilde{q}\})$ can be written as,

$$\mathcal{H}(\{\tilde{q}\}) = \sum_{\vec{n}_1, \vec{n}_2} g_2(\vec{n}_1, \vec{n}_2) \tilde{q}_{\vec{n}_1} \tilde{q}_{\vec{n}_2} + \dots \quad (\text{A13})$$

where higher-body (*i.e.*, 4-, 6-, ... body) terms are neglected for simplicity, which corresponds to the Villain’s approximation. The two-body interaction $g_2(\vec{n}_1, \vec{n}_2)$ is essentially the same as the spin-wave Green’s function,

$$\begin{aligned} g_2(\vec{n}_1, \vec{n}_2) &\equiv \sum_{\vec{k}} \frac{e^{i\vec{k} \cdot (\vec{n}_1 - \vec{n}_2)}}{4 - 2(\cos(k_x) + \cos(k_y))} \\ &\simeq \frac{1}{2\pi} \int_{\pi/L}^{\pi} dk k \frac{e^{ik|n_1 - n_2|}}{k^2}. \end{aligned} \quad (\text{A14})$$

In the first equation, the summation over all possible wavevectors $\vec{k} = (k_x, k_y)$ allowed in the periodic system of size $L \times L$ is taken. The Green’s function behaves at large distances as,

$$g_2(\vec{n}_1, \vec{n}_2) \approx 2\pi \ln(|\vec{n}_1 - \vec{n}_2|) + 2\pi \ln(2\sqrt{2}e^\gamma), \quad (\text{A15})$$

where γ is Euler’s constant while

$$g_2(\vec{n}, \vec{n}) \approx 2\pi \ln(L) + 2\pi \ln(2\sqrt{2}e^\gamma), \quad (\text{A16})$$

which is the bare vortex core energy of a finite sized system of size L .

Within the Villain’s approximation, we find,

$$\begin{aligned} V &= \left. \frac{\partial^2 F}{\partial m^2} \right|_{m=0} \\ &= g_2(\vec{0}, \vec{0}) - \beta \sum_{\vec{n}, \vec{n}'} g_2(\vec{0}, \vec{n}) g_2(\vec{0}, \vec{n}') (\langle \tilde{q}_{\vec{n}} \tilde{q}_{\vec{n}'} \rangle_c - \langle \tilde{q}_{\vec{n}} \rangle_c \langle \tilde{q}_{\vec{n}'} \rangle_c). \end{aligned} \quad (\text{A17})$$

The first term on the r.h.s of the last equation is obviously the vortex creation energy which generally scales as $c(0) + v(0) \ln(L)$ with a ‘bare’ vorticity modulus at zero temperature $v(0) = 2\pi$ and a constant $c(0) = 2\pi \ln(2\sqrt{2}e^\gamma)$. The second term would be interpreted as a ‘screening’ term due to thermal fluctuations of other charges. On general grounds, we speculate that the same scaling holds at finite temperatures below the critical temperature T_s ,

$$V = c(T) + v(T) \ln(L), \quad T < T_s, \quad (\text{A18})$$

with a temperature-dependent vorticity modulus $v(T)$. Above T_s , we have $v(T) = 0$ in the thermodynamic limit $L \rightarrow \infty$.

The obtained expression of V , Eq. (A17), should be compared with the corresponding expression for the helicity modulus which is given by [16, 41],

$$\Upsilon = 1 - \frac{\beta}{N} \sum_{\vec{n}, \vec{n}'} g_2(\vec{n}, \vec{n}') (\langle \tilde{q}_{\vec{n}} \tilde{q}_{\vec{n}'} \rangle_c - \langle \tilde{q}_{\vec{n}} \rangle_c \langle \tilde{q}_{\vec{n}'} \rangle_c). \quad (\text{A19})$$

-
- [1] J. Villain, *J. of Phys. C: Solid State Phys.*, **10** 4793 (1977).
[2] S. Teitel and C. Jayaprakash, *Phys. Rev. B* **27**, 598 (1983).
[3] S. Miyashita and H. Shiba, *J. Phys. Soc. Jpn.* **53**, 1145 (1984).
[4] H. S. J. van der Zant, H. A. Rijken, and J. E. Mooij, *J. Low. Temp. Phys.*, **82** 67 (1991).
[5] P. Martinoli and Ch. Leemann, *J. Low Temp. Phys.* **118**, 699 (2000).
[6] N. D. Mermin and H. Wagner, *Phys. Rev. Lett.* **17**, 1133 (1966).
[7] J. M. Kosterlitz and D. J. Thouless, *J. of Phys. C: Solid State Phys.* **6** 1181 (1973).
[8] For a recent review, see H. Kawamura, *J. Phys. Soc. Jpn.* **79** (2010) 011007.
[9] D. H. Lee, J.D. Joannopoulos, J. W. Negele and D. P. Landau, *Phys. Rev. Letters* **52**, 433 (1984); *Phys. Rev. B* **33**, 450 (1986).
[10] J. M. Thijssen and H. J. F. Knops, *Phys. Rev. B* **42**, 2438 (1990).
[11] J. Lee, J. M. Kosterlitz and E. Granato, *Phys. Rev. B* **43**, 11531 (1991).
[12] E. Granato and M. P. Nightingale, *Phys. Rev. B* **48**, 7438 (1993).
[13] S. Lee and K. -C. Lee, *Phys. Rev. B* **49**, 15184 (1994).
[14] G. Ramirez-Santiago and J. V. José, *Phys. Rev. Lett.* **68**, 1224 (1992); *Phys. Rev. B* **49**, 9567 (1994).
[15] M. P. Nightingale, E. Granato and J. M. Kosterlitz, *Phys. Rev. B* **52**, 7402 (1995).
[16] P. Olsson, *Phys. Rev. Letters* **75**, 2758 (1995); *Phys. Rev. B* **55**, 3585 (1997).
[17] H. -J. Xu and B. W. Southern, *J. Phys. A* **29**, L133 (1996).
[18] S. Lee and K. -C. Lee, *Phys. Rev. B* **57**, 8472 (1998).
[19] E. H. Boubcheur and H. T. Diep, *Phys. Rev. B* **58**, 5163 (1998).
[20] Y. Ozeki and N. Ito, *Phys. Rev. B* **68**, 054414 (2003).
[21] Martin Hasenbusch, Andrea Pelissetto, and Ettore Vicari, *Phys. Rev. B* **72**, 184502 (2005).
[22] Martin Hasenbusch, Andrea Pelissetto, and Ettore Vicari, *J. Stat. Mech.*, P12002 (2005).
[23] J. M. Thijssen and H. J. F. Knops, *Phys. Rev. B* **37**, 7738 (1988).
[24] G. S. Grest, *Phys. Rev. B* **39**, 9267 (1989).
[25] J. -R. Lee, *Phys. Rev. B* **49**, 3317 (1994).
[26] P. Minnhagen, *Phys. Rev. B* **32**, 7548 (1985).
[27] E. Granato and D. Dominguez, *Phys. Rev. B* **71**, 094521 (2005).
[28] S. E. Korshunov, *Phys. Rev. Lett.* **88**, 167007 (2002).
[29] P. Olsson and S. Teitel, *Phys. Rev. B* **71**, 104423 (2005).
[30] L. Capriotti, R. Vaia, A. Cuccoli and V. Tognetti, *Phys. Rev. B* **58**, 273 (1998).
[31] S. Lee, K. -C. Lee and J. M. Kosterlitz, *Phys. Rev. B* **56**, 340 (1997).
[32] J. Lee, E. Granato, and J. M. Kosterlitz, *Phys. Rev. B* **44**, 4819 (1991).
[33] M. Y. Choi and D. Stroud, *Phys. Rev. B* **32**, 5773 (1985).
[34] E. Granato and J. M. Kosterlitz and J. Poulter, *Phys. Rev. B* **33**, 4767 (1986).
[35] G. S. Jeon, S. Y. Park and M. Y. Choi, *Phys. Rev. B* **55**, 14088 (1997).
[36] H. Kawamura and M. Kikuchi, *Phys. Rev. B* **47**, 1134 (1993).
[37] B. W. Southern and H. -J. Xu, *Phys. Rev. B* **52**, R3836 (1995).
[38] S. Grosse Pawig and K. Pinn, *Int. J. Mod. Phys. C* **9**, 727 (1998).
[39] D. R. Nelson and J. M. Kosterlitz, *Phys. Rev. Lett.* **39**, 1201 (1977).
[40] J. V. José, L. P. Kadanoff, S. Kirkpatrick, D. R. Nelson, *Phys. Rev. B* **16**, 1217 (1977).
[41] P. Minnhagen, *Rev. of Mod. Phys.* **59**, 1001 (1987).
[42] P. Minnhagen, *Phys. Rev. Lett.* **54**, 2351 (1985); *Phys. Rev. B* **32**, 3088 (1985).